Dimesitylborane as Electron Accepting Unit in High Performance Yellow Single-Layer Phosphorescent Organic Light Emitting Diode

Clément Brouillac, Fabien Lucas, Denis Ari, Christophe Lebreton, Olivier Jeannin, Joëlle Rault-Berthelot, Cassandre Quinton, Emmanuel Jacques, Cyril Poriel

NANO · MICRO small
www.small-journal.com

Dimesitylborane as Electron Accepting Unit in High Performance Yellow Single-Layer Phosphorescent Organic Light Emitting Diode

*Clément Brouillac, Fabien Lucas, Denis Ari, Christophe Lebreton, Olivier Jeannin, Joëlle Rault Berthelot, Cassandre Quinton, Emmanuel Jacques, and Cyril Poriel**

A new host material for Single-Layer Phosphorescent Organic Light-Emitting Diodes (SL-PhOLED) is reported, namely SPA-2-FDMB, using the dimesitylborane (DMB) fragment as an acceptor unit. The molecular design is constructed on the general donor-*spiro*-acceptor architecture, which consists of connecting, via a *spiro* bridge, a donor and an acceptor units in order to avoid strong interaction between them. The DMB fragment is known for many electronic applications (notably Aggregation-Induced Emission) but has not been used yet for SL-PhOLED applications. This appears particularly interesting, as the development of this simplified technology has shown that only a few electron-accepting fragments such as diphenylphosphine oxide can provide high-performance devices. Herein, the yellow-emitting SL-PhOLED using SPA-2-FDMB as host presents an External Quantum Efficiency of 8.1% (Current Efficiency of 24.9 cd.A^{-1}) with a low threshold voltage of 2.6 V. As SPA-2-FDMB presents a sharp HOMO/LUMO difference, the good matching of HOMO and LUMO energy levels with the Fermi level of the electrodes is responsible for these performances. The low LUMO level of −2.61 eV also appears particularly important. These performances are, to date, the highest reported for a yellow/orange-emitting SL-PhOLED and show the potential of DMB unit in the single-layer technology.

1. Introduction

Since the first proof-of-concept of Organic Light-Emitting Diodes (OLED) in 1987,[1] this technology has enormously evolved and is now taking part in various commercially available devices such as smartphones, laptops, tablets and televisions. The recent fantastic developments in foldable and rollable display screens result from this technology. Phosphorescent OLEDs (PhOLED) are the second generation of OLEDs[2–6] and the most widely used today. A PhOLED uses an emissive layer (EML) composed of a host:guest blend. In this system, a phosphorescent emitter (guest) is dispersed into an organic semiconductor (host). In the last decade, impressive improvements in terms of efficiency were achieved thanks to precise molecular designs of the host material and efficient device engineering techniques. These engineering works, principally based on an adjustment of the electron/hole transporting/blocking layers, have allowed to maximize the efficiency of the PhOLED stack and to date all the most efficient PhOLEDs reported in red, green and blue (RGB) emissions are constructed on a multi-layer (ML) stack.[7–16] Despite very efficient, a ML stack increases the device cost and complexity of the technology rendering it, in consequence, poorly sustainable. However, sustainability must be a central concern nowadays and simplifying the PhOLED stack by decreasing the number of organic layers is therefore an important challenge for the reduction of both the

C. Brouillac, D. Ari, O. Jeannin, J. Rault Berthelot, C. Quinton, C. Poriel
Univ Rennes
CNRS
ISCR-UMR CNRS 6226
Rennes F-35000, France
E-mail: cyril.poriel@univ-rennes.fr

The ORCID identification number(s) for the author(s) of this article can be found under https://doi.org/10.1002/smll.202405312

DOI: 10.1002/smll.202405312

F. Lucas
LPICM
CNRS
Ecole Polytechnique
IPParis
Palaiseau 91128, France

C. Lebreton, E. Jacques
Univ Rennes
CNRS
IETR-UMR CNRS 6164
Rennes F-35000, France

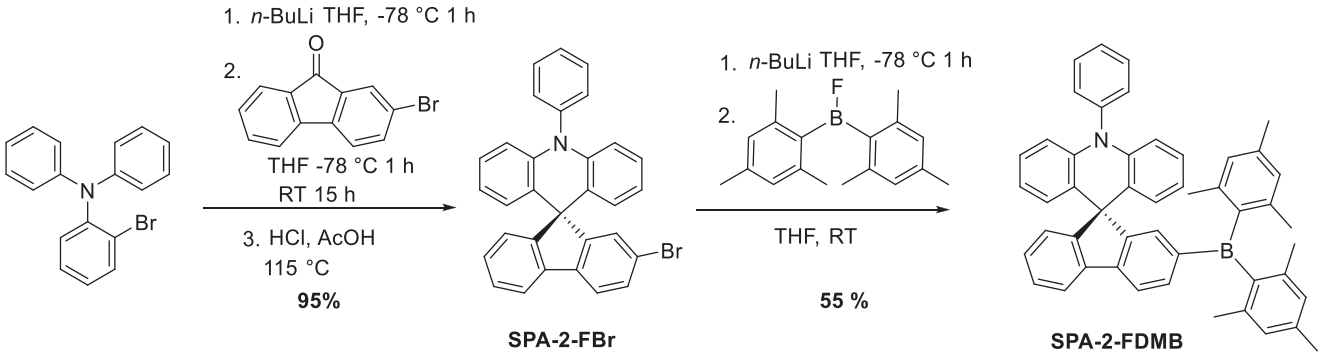

Scheme 1. Synthetic pathway of **SPA-2-FDMB**.

production cost and the environmental footprint. Such a simplified device called Single-Layer OLED has been investigated for a long time by many research groups and for all the generations of emitters, that is, fluorescent,[17–19] phosphorescent[20–28] or thermally activated delayed fluorescent (TADF).[29–31] Single-Layer Phosphorescent OLEDs (SL-PhOLEDs) have been particularly investigated in recent years as the performance of these devices has started to significantly increase. The key to success in SL-PhOLEDs was linked to the performance of the host material used and its capability to gather numerous important electronic properties. In such a device, the EML alone should warranty, in addition to the emission of light, the efficient electron and hole transporting and blocking capabilities, usually provided by the intermediate functional layers. The molecular design of the host, usually built with the connection of electron-rich and electron-poor units, is then crucial in this simplified technology. The nature of the electron-withdrawing fragment is particularly important as the flow of electrons in such a device is crucial notably to induce a good charge balance. In the SL-PhOLED literature, the diversity of electron-withdrawing units used in high-efficiency devices is very poor and the diphenylphosphine oxide fragment is almost the only efficient one.[21–26,32–38] However, it is known that this fragment, despite its very high efficiency displays an instability originating from the weak C—P bond.[39] Therefore, developing other efficient acceptor units for SL-PhOLED appears as a new challenge in the field.

In this work, we report a new host material for SL-PhOLED, namely **SPA-2-FDMB**, using the dimesitylborane (DMB) fragment as an acceptor unit. The molecular design is constructed on the general donor-*spiro*-acceptor architecture,[40] which consists of connecting, via a *spiro* bridge, a donor and an acceptor unit in order to avoid strong interaction between them. The donor used herein is the famous phenylacridine (PA) fragment found in the design of many high-efficiency hosts[22,23] and fluorescent emitters.[41–43] The DMB fragment is known for its AIE (Aggregation Induced Emission) behaviour,[44–54] and has been incorporated in several fluorophores for OLEDs[55] with notably Thermally Activated Delayed Fluorescent (TADF) properties[56–62] or as host for phosphors in ML-PhOLEDs.[63–67] However, as far as we know, DMB fragment has never been introduced in a host material for an SL-PhOLED and the quest toward novel high-efficiency acceptor fragment is undoubtedly important for the future of these devices.

In recent years, significant progresses have been made in SL-PhOLEDs performances and very high External Quantum Efficiency (EQE), higher than 20% in some rare cases, for green and blue devices have been reached.[20,24,34] The first high performance white-emitting devices have even been reported recently with a very high EQE of 24%, obtained by the superposition of two EMLs.[25] However, yellow/orange SL-PhOLEDs are almost absent from the literature and as far as we know only four examples have been reported to date.[68–71] As the development of new acceptor fragments for SL-PhOLEDs is a new challenge to address, we design herein a new DMB-based host material for a yellow/orange SL-PhOLED. The phosphor used is a yellow/orange emitter called PO-01. This dopant has been incorporated in SL-PhOLED only one time and the best current efficiency (CE) reported to date is 16 cd.A^{-1}.[68] In the present work, the yellow-emitting SL-PhOLED presents an EQE of 8.1%, a CE of 24.9 cd.A^{-1} and a Power Efficiency (PE) of 10.6 lm W^{-1}. As the host material presents a narrow HOMO/LUMO difference, a very low threshold voltage (V_{ON}) of 2.6 V is reached, due to a good matching of HOMO and LUMO energy levels with respect to the Fermi level of the electrodes. The low LUMO level of −2.61 eV is thus particularly important herein. These performances are, as far as we know, the highest reported for a yellow/orange-emitting SL-PhOLED and show the potential of DMB unit in the single-layer technology.

2. Results and Discussion

SPA-2-FDMB was synthesized in a very simple two-step approach with a high global yield of 52% (**Scheme 1**). The platform **SPA-2-FBr** was first obtained, with 95% yield, via a nucleophilic addition reaction of 2-bromofluorenone with the lithiated intermediate triphenylamine providing the corresponding fluorenol, further cyclized in a 10% mixture HCl/AcOH. The last step is the nucleophic addition of the corresponding lithiated platform from **SPA-2-FBr** on dimesitylboron fluoride to form the targeted compound, **SPA-2-FDMB**, in 55% yield.

2.1. Structural Properties

The structural arrangement of **SPA-2-FDMB** (CCDC 2 359 045) obtained by X-ray diffraction is depicted in **Figure 1**. The most

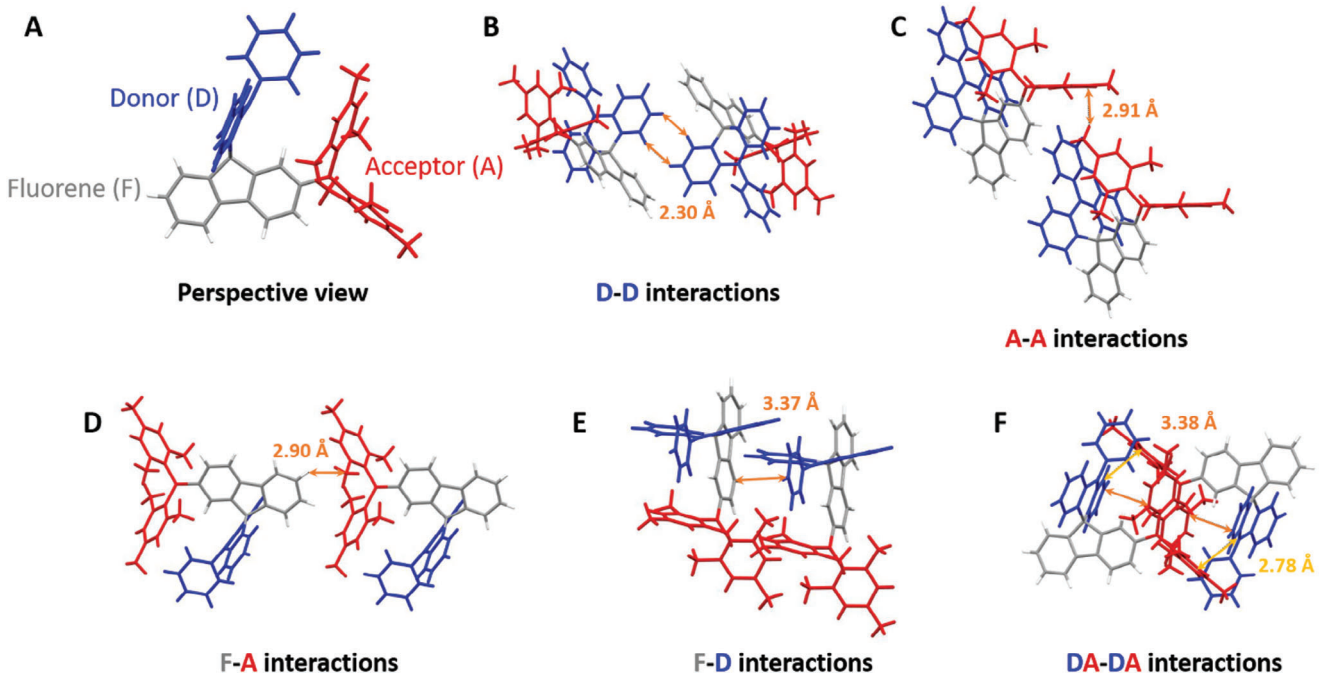

Figure 1. Molecular structure from single cristal X-ray diffraction of **SPA-2-FDMB** (2 359 045), A) the perspective view, B) the donor-donor packing interactions, C) the acceptor–acceptor packing, D) the fluorene-acceptor interactions, E) the fluorene-donor interactions, F) the donor-acceptor interactions

important structural feature is the position of the *spiro* connected phenylacridine. Indeed, the dihydroacridine unit is significantly tilted toward the DMB (Figure 1A). In addition, the two external benzene rings of the dihydroacridine moiety form an angle of 20.2°, showing the strong deformation of this fragment. These two characteristics are different to those previously reported for other *spiro*-connected phenylacridine compounds previously reported in the literature.[72]

Many C—C, C—H and H—H short distances drive the packing diagram of **SPA-2-FDMB**. It is interesting to note that all the different fragments of the molecules are involved in these interactions, namely the donor part, phenylacridine, the acceptor part, dimesitylborane and the linker, fluorene (Figure 1B–F).

2.2. Electrochemical Properties

The electrochemical behaviour has been investigated by cyclic voltammetry (CV) in dichloromethane for oxidation and in dimethylformamide for reduction, potentials are given versus a saturated calomel electrode (SCE). In both oxidation and reduction, **SPA-2-FDMB** presents a first reversible wave at respectively 0.98 and −1.82 V showing the stability of the radical cation and radical anion (**Figure 2**). This is a very interesting behaviour especially for bipolar charge transport, a key feature in SL-PhOLEDs. The HOMO, determined from the onset potential of the first oxidation wave, has been evaluated at −5.28 eV (**Table 1**). Molecular modelling shows that the HOMO is exclusively spread out on the phenylacridine moiety translating a first electron transfer located on this unit (Figure 2-right). We can note that the energy of the HOMO level is in accordance with that of its analogue **SPA-2-FPOPh$_2$**, previously reported in literature,[21] possessing a diphenylphosphine oxide at the C2 position (HOMO at −5.33 eV). **SPA-2-FPOPh$_2$** will be used in this study as a model compound (see molecular structure in ESI) in order to highlight the impact of the DMB unit on the physico-chemical properties. These similar HOMO energy levels show the good separation between the electron-rich and electron-poor units thanks to the *spiro* carbon, which avoids interactions between them. The LUMO level, determined from the onset potential of the first reduction wave, has been measured very low at −2.61 eV (Figure 2-left). The LUMO is not exclusively spread out on the acceptor unit, that is, DMB, but dispersed on both the fluorene and the DMB fragments (Figure 2-right). This shows that the boron atom allows a more efficient π-delocalization than the phosphorus atom. Thanks to its empty p orbitals and the resulting strong accepting electronic properties, the DMB unit allows to depress the LUMO of **SPA-2-FDMB** by 0.38 eV compared to that of its analogue **SPA-2-FPOPh$_2$** (−2.23 eV). This shows the stronger electron-withdrawing capability of the DMB unit compared to diphenylphosphine oxide. Theoretical calculations also provide the same trend for the HOMO and LUMO energy levels −5.32 eV (vs −5.27 eV for **SPA-2-FPOPh$_2$**) and −2.04 eV (vs −1.60 eV for **SPA-2-FPOPh$_2$**) respectively. Thanks to this design, the electrochemical gap (ΔE_{EL}) of **SPA-2-FDMB** is very narrow (2.67 eV). In addition to a good alignment of the HOMO and LUMO, a narrow bandgap can considerably increase the charges injection in the SL-PhOLED, leading to low threshold voltage. This is a key feature in single-layer technology as both kind of charge carriers needs to be directly injected into the EML. This is discussed below.

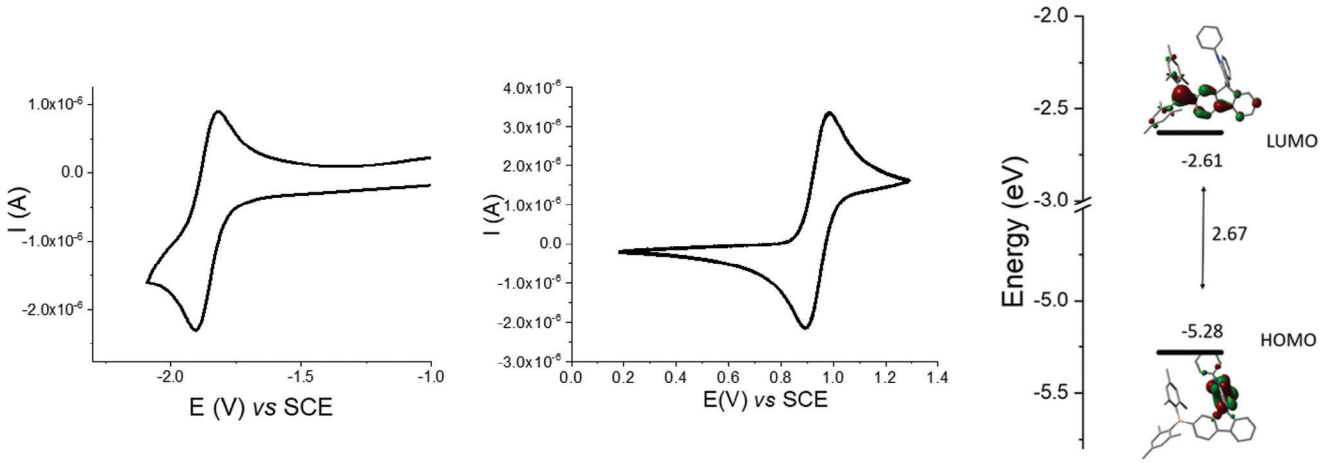

Figure 2. Cyclic voltammetry recorded on Pt working electrode in reduction (left, DMF + Bu_4NPF_6 0.1 M, sweep-rate 100 mV s^{-1}) and in oxidation (middle, DCM + Bu_4NPF_6 0.2 M, sweep-rate 100 mV s^{-1}) of **SPA-2-FDMB** Representation of HOMO/LUMO calculated by TD-DFT (B3LYP/6-311+G(d,p)) (isovalue 0.04 [ebohr^{-3}]$^{1/2}$) and the energy levels obtained by cyclic voltammetry (Right).

2.3. Photophysical Properties

The UV–Vis absorption and emission spectra of **SPA-2-FDMB** have been recorded in cyclohexane at room temperature (**Figure** 3A). The optical properties are summarized in Table 1. The intense band at 347 nm can be attributed from TD-DFT calculations to two different transitions (HOMO-1→LUMO and HOMO-2→LUMO) modelled respectively at 357 and 359 nm and all localized on the acceptor part (fluorene and DMB fragment, **Figure** 4C). It is interesting to note that there is an important energy difference (0.73 eV) between the HOMO (localized on the electron-rich PA unit) and the HOMO-1 (localized on the fluorene core) whereas the difference between HOMO-1 and HOMO-2 (localized on the DMB unit) is weak (0.17 eV). As classically observed for D-*spiro*-A compound, the HOMO→LUMO transition is forbidden (f = 0.000) due to the spatial separation of the HOMO localized on the donor part and the LUMO localized on the acceptor part by the *spiro* carbon (Figure 2-right).

The emission spectrum shows a single band with a maximum of 433 nm. Compared to its analogue **SPA-2-FPOPh$_2$**, the maximum of emission (λ_{em}) of **SPA-2-FDMB** is significantly red-shifted (λ_{em} = 433 nm vs λ_{em} = 402 nm) due to the higher electron withdrawing capability of the DMB fragment compared to diphenylphosphine oxide fragment in accordance with above mentioned results.

We next study the polarity of the excited states by measuring emission spectra in solvents with different polarities. An impressive red shift of 111 nm appears when the polarity of the solvent increases, from 433 nm in apolar cyclohexane to 544 nm in highly polar acetonitrile (Figure 3B). This intense solvatochromic effect highlights a strong photoinduced intramolecular charge transfer (ICT). The differences (Δμ) between the dipole moment at the ground state (μ) and at the first excited state (μ*) have been estimated using the Lippert-Mataga formalism (see ESI, Figure S10 and Tables S1 and S3, Supporting Information).[73] A Δμ of 20.5 D have been experimentally measured for **SPA-2-FDMB** (the dipole moment at the ground state has been obtained by DFT calculations, 1.4 D), see ESI for details about the calculations). The μ* of **SPA-2-FDMB** can be then estimated at 21.9 D. Thus, the significant solvatochromic effect and the corresponding high Δμ translate a strong photoinduced ICT in accordance with the strong electron-withdrawing effect of DMB core. In comparison, a lower Δμ of 16.0 D is measured for **SPA-2-FPOPh$_2$** (see ESI, Figures S6 and S10 and Tables S2 and S3, Supporting Information) in accordance with a weaker electron accepting unit.

The quantum yield of **SPA-2-FDMB** is null (f = 0.000) due to the forbidden $S_0 \rightarrow S_1$ transition induced by the spatial separation of HOMO and LUMO. It is a well-known characteristic in bipolar host materials.

Table 1. Photophysical and electrochemical properties of **SPA-2-FDMB**.

	λ_{abs} [nm][a]	λ_{em} [nm][a,b]	QY[a,b,c]	λ_{em} (77 K) [nm][d]	E_T [eV][e]	τ_p [s][d]	τ_f [ns][a,b]	E_{ox} [V][f,g]	E_{red} [V][f,h]	HOMO [eV][i]	LUMO [eV][i]	ΔE_{EL} [eV][j]
SPA-2-FDMB	263 334 347	433	0.01	478	2.59	4.5	6.89	0.98 1.72 1.97 2.17	−1.82	−5.28	−2.61	2.67

[a] in cyclohexane at RT; [b] λ_{exc} = 310 nm; [c] Quantum yield (QY) determined with sulfate quinine in 1 M H_2SO_4 as the reference; [d] in 2-MeTHF at 77 K, λ_{exc} = 350 nm; [e] from first phosphorescence peak E (eV) = 1239.84 / λ; [f] versus SCE; [g] in DCM; [h] in DMF; [i] from electrochemical data; [j] ΔE_{El} = |HOMO-LUMO|.

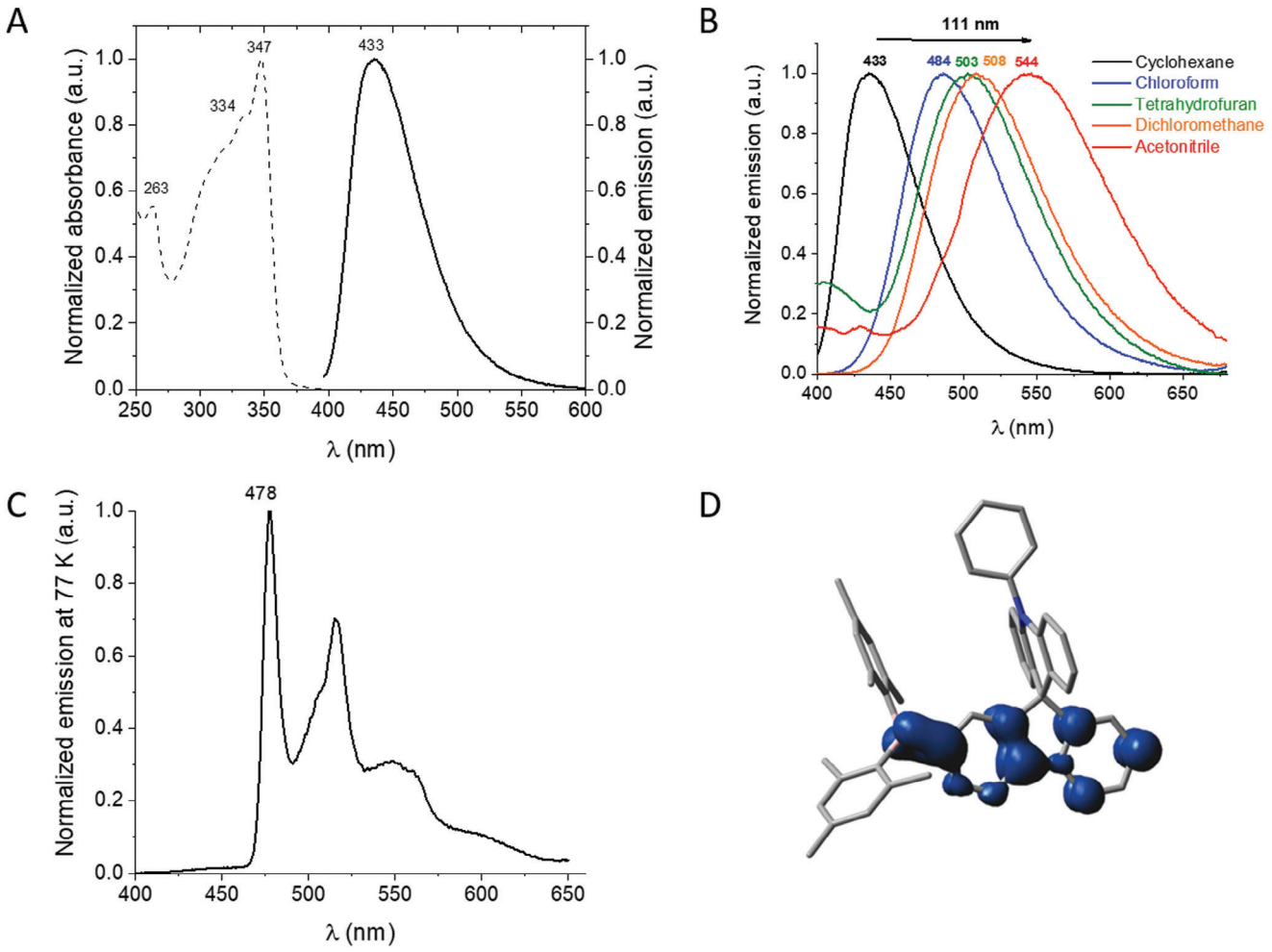

Figure 3. A) UV–vis absorption and emission spectra in cyclohexane (λ_{exc} = 310 nm) of **SPA-F-2-DMB**. B) Normalized emission spectra at room temperature in different solvents. C) Normalized emission spectra at 77 K in 2-MeTHF (λ_{exc} = 330 nm). D) Triplet spin density distribution (TD-DFT, B3LYP/6-311+g(d,p), isovalue 0.004 [ebohr^{-3}]$^{1/2}$).

At 77 K, the emission spectrum shows phosphorescence contributions with a first band at 478 nm leading to a triplet state energy level (E_T) of 2.59 eV. A lifetime of 4.5 s was measured in accordance with a phosphorescence emission (see Figure S4, Supporting Information). The E_T, compared to that of **SPA-2-FPOPh$_2$** (E_T = 2.76 eV), is lower due to a higher conjugation between the carbon atom of the fluorene and the boron atom of the dimesitylborane than the phosphorus atom of the phosphine oxide. Indeed, the spin density of the triplet state of **SPA-F-2-DMB** is localized on both the fluorene and the boron atom while it is localized only on the fluorene for **SPA-2-FPOPh$_2$**,[21] showing a longer π-conjugation pathway, providing in turn a lower E_T (Figure 3D).

2.4. Thermal Properties

As the stability of the host material is a key consideration not only for device stability but also for its fabrication by sublimation, the thermal properties have been studied using differential scanning calorimetry (DSC) and thermogravimetric analysis (TGA) (Figure 4). The decomposition temperature T_d (5% mass loss) is recorded at 315 °C and the glass transition temperature (T_g) is detected at 132 °C. These temperatures are sufficiently high to allow thermal evaporation and stability of the electroluminescence without any phase transition. Compared to **SPA-2-FPOPh$_2$**, the T_g is almost identical (143 °C for **SPA-2-FPOPh$_2$**) showing that the DMB fragment gives similar thermal properties than the bulky diphenylphosphine. Nevertheless, unlike **SPA-2-FPOPh$_2$**, note that the DMB unit leads to the presence of a crystallization temperature (T_c) detected at 240 °C.

2.5. Charges Transport Properties

One of the most important parameters in SL-PhOLED is having a good balance between the transport of electrons and holes in order to favour the recombination of charges within the centre of the emissive layer (EML). To measure both hole and electron charge carrier mobilities, measuring space charged

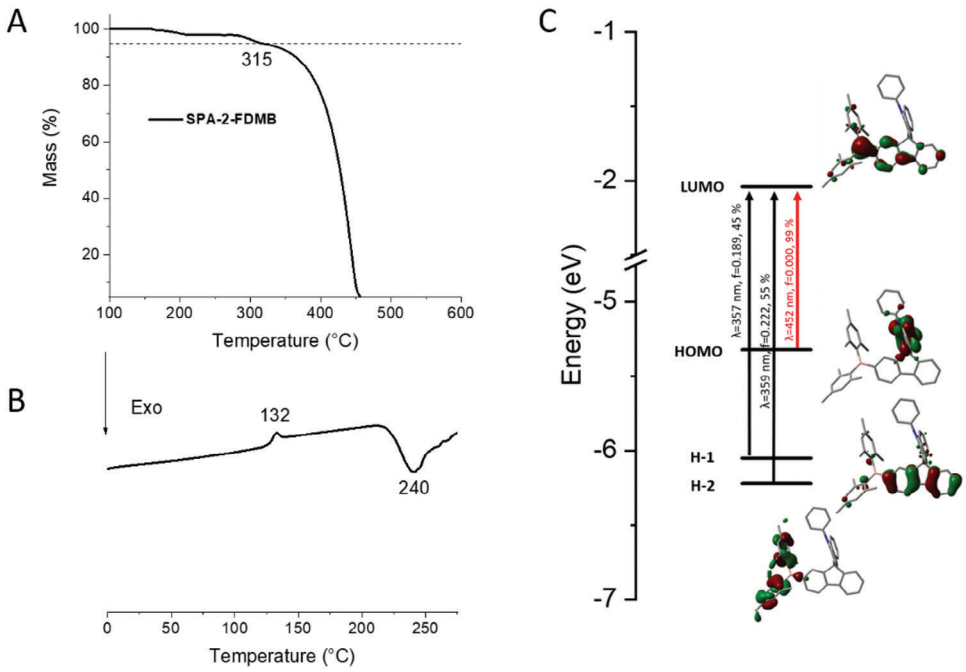

Figure 4. A) TGA and B) DSC (2nd heating only) traces of **SPA-2-FDMB**, and C) representation of the energy levels and the main molecular orbitals involved in the electronic transitions obtained by TD-DFT, B3LYP/6–311+G(d,p), shown with an isovalue of 0.04 $[ebohr^{-3}]^{1/2}$. For clarity purposes, only the major contribution of each transition is shown (see Supporting Information for details).

limiting current (SCLC) into vertical two-terminal devices is the most appropriate. Herein, electron-only and hole-only devices have been fabricated. The hole (μ_h) and electron (μ_e) mobilities have been estimated to be respectively 1.48×10^{-5} and 1.41×10^{-10} $cm^2\ V^{-1}\ s^{-1}$ for **SPA-2-FDMB** (**Figure 5**). One can note that the electrons mobility is five decades lower than the holes mobilities. Despite the high electron withdrawing DMB fragment, the electrons mobility remains surprisingly very weak. The holes and electrons carriers densities have been evaluated at respectively 1.7×10^{17} and 4.7×10^{15} cm^{-3} showing a higher number of holes in the host compared to the number of electrons. However, the presence of the phosphor in the EML can contribute to more balance in the charge flow as shown in previous works.[20,24]

3. Single-Layer Phosphorescent OLED

Finally, **SPA-2-FDMB** has been used as a host matrix doped by PO-01 forming thus the EML of the SL-PhOLED. PO-01 is a yellow-orange phosphorescent emitter, which has been used, to the best of our knowledge, only one time in SL-PhOLED.[68] The highest performance to date has been reported with the famous carbazole-based host, 4,40-bis(carbazol-9-yl)biphenyl (**CBP**), with a maximum current efficiency (CE) of 16.34 cd A^{-1} (no EQE was reported).[68]

First, the iridium complex PO-01 has been studied in order to determine its electronic properties and particularly its HOMO and LUMO energy levels and E_T. Thus, in dichloromethane at room temperature, the E_T of PO-01 has been evaluated at 2.22 eV

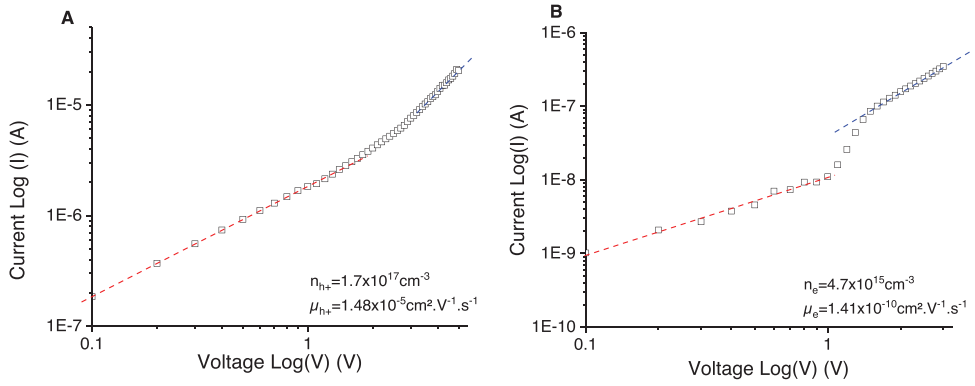

Figure 5. Thickness-scaled current-voltage characteristics of **SPA-2-FDMB** hole-A) and electron-only B) SCLC devices.

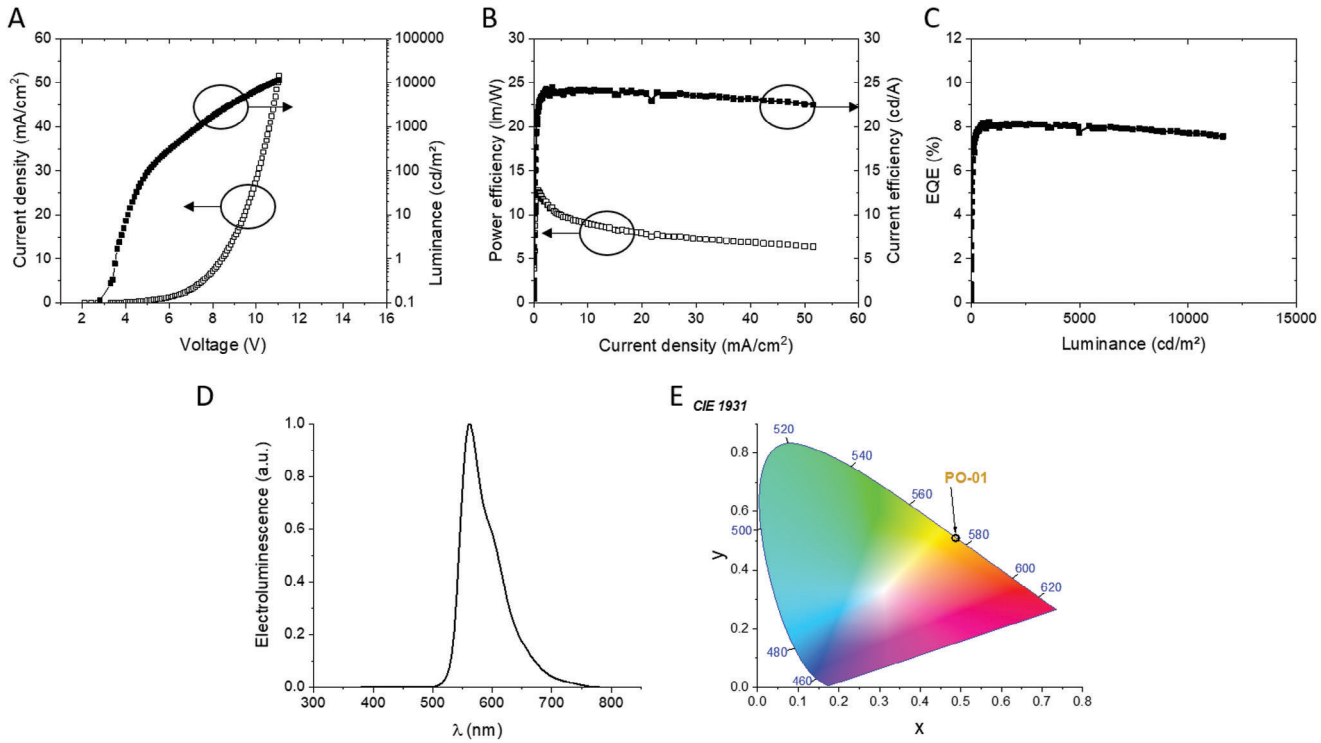

Figure 6. SL-PhOLED characteristics using **SPA-2-FDMB** as host material and PO-01 as phosphorescent emitter. A) Current density (mA.cm^{-2}) and luminance (cd.m^{-2}) as a function of the voltage (V). B) Current efficiency (cd.A^{-1}, filled symbols) and power efficiency (lm.W^{-1}, empty symbols) as a function of the current density (mA.cm^{-2}). C) Roll-off Efficiency: EQE (%) as a function of the luminance (cd.m^{-2}). D) Normalized electroluminescent spectrum at 10 mA.cm^{-2} and E) Corresponding CIE diagram.

from the maximum of first emission peak (λ = 558 nm), Figure S9 (Supporting Information). At 77 K, in a frozen 2-MeTHF matrix (same conditions as those used to measure the E_T of **SPA-2-FDMB**), there is a blue shift of the emission spectra (λ = 545 nm), Figure S9 (Supporting Information) due to the decrease of molecular motions and the E_T is hence slightly increased at 2.28 eV. The HOMO/LUMO energy levels of PO-01 have also been evaluated by electrochemical analyses in solution −5.03/−2.41 eV (in CH_2Cl_2 +Bu_4NPF_6 0.2 M, see CV in) at (Figures S11–S14, Supporting Information). These data are particularly interesting in interpreting the device performance presented below.

The SL-PhOLED structure used in this work is the following: ITO/PEDOT:PSS (40 nm)/EML (Host+Guest 10% wt.) (100 nm)/LiF (1.2 nm)/Al (100 nm). Thus, the ITO anode is not neat but covered by a thin PEDOT:PSS layer to allow a better organization of the interface with the EML and a decrease of the anode work function.[74] Similarly, a thin layer of LiF, known to reduce the work function of metal electrodes and significantly enhancing charge carriers injection, was deposited onto Aluminum.[75] First, the electroluminescent spectrum of the SL-PhOLED exhibits a yellow emission with CIE coordinates of 0.49;0.51 arising exclusively from PO-01, showing an efficient energy transfer cascade (**Figure 6D**). The electroluminescent spectrum is very similar to the thin film photoluminescent spectrum recorded on a mixture of **SPA-2-FDMB** (w = 90%) and PO-01 (w = 10%), Figure S16, Supporting Information) revealing that PO-01 is the unique emitter in the device.

The yellow SL-PhOLED reaches a maximum EQE of 8.1%, equivalent to a CE of 24.9 cd.A^{-1} and to a PE of 10.6 lm.W^{1} (at 4.2 mA.cm^{-2}, **Table 2**). The best device reaches a high maximum luminance of 21 610 cd.m^{-2} at 150 mA.cm^{-2}. These performances are, as far as we know, the highest reported for a yellow SL-PhOLED and reveal the efficiency of the DMB unit for SL-PhOLED applications. Remarkably, at 10 mA.cm^{-2}, the EQE remains stable, 7.9% (corresponding CE/PE of 24.3 cd.A^{-1}/9.0 lm.W^{1}) showing a very low-efficiency roll-off, translating an excellent stability of the device at high current densities. For practical applications of the OLED technology, the stability of the performance at high current densities (i.e., low-efficiency roll-off) is at least as important as the performances themselves. Even at higher current densities as presented in Figure 6, the CE remains almost identical to the initial value. In addition, note that at 10 000 cd.m^{-2}, EQE remains as high as ca 8% (Figure 6C).

All these characteristics show the excellent stability of the present device. The threshold voltage (V_{on}), which is usually, in this simplified technology, a real issue appears herein as low as 2.6 V showing excellent charge injection. This is due to the very short gap of **SPA-2-FDMB** and the very good matching between the HOMO and LUMO level of **SPA-2-FDMB** (−5.28/−2.61 eV) and the Fermi levels of the anode (ITO/PEDOT-PSS, −5.1 eV) and cathode (LiF/Al, −2.8 eV) respectively, which are responsible for facilitating efficient hole and electron injections. One can also note that the LUMO of **SPA-2-FDMB** (−2.61 eV) is particularly

Table 2. SL-PhOLED data of **SPA-2-FDMB** as host with 10% of PO-01 as dopant.

	V_{ON} [V]	EQE [%]	CE [cd.A^{-1}]	PE [lm.W^{-1}]	EQE [%]	CE [cd.A^{-1}]	PE [lm.W^{-1}]	L [cd.m^{-2}]	CIE Coordinates (x ; y)
		At 10 mA.cm^{-2}			Max (at J [mA.cm^{-2}])				At 10 mA.cm^{-2}
SPA-2-FDMB/ PO-01 (10%)	2.6	7.9	24.3	9.0	8.1 (4.2)	24.9 (4.2)	10.6 (4.2)	21 610 (150)	0.49; 0.51

well adapted to that of PO-01 (−2.41 eV) insuring an efficient relay for the electron injection from the LiF/Al cathode (2.8 eV).

4. Conclusion

In summary, we report a new host material for simplified SL-PhOLEDs, incorporating for the first time a DMB core as electron-accepting unit. Thanks to this DMB unit, the corresponding host **SPA-2-FDMB** displays notably a very low LUMO energy level of great interest for electron injection in SL-PhOLED. The yellow-emitting SL-PhOLED incorporating **SPA-2-FDMB** as host presents an EQE of 8.1%, a CE of 24.9 cd.A^{-1} and a PE of 10.6 lm.W^{-1}. The device also possesses a very low threshold voltage of 2.6 V induced by the excellent matching of HOMO and LUMO energy levels of **SPA-2-FDMB** with the Fermi level of the electrodes and a narrow bandgap. To be the best of our knowledge, these performances are the highest reported to date for a yellow/orange-emitting SL-PhOLED. The DMB fragment appears then as an interesting building unit to significantly depress the LUMO energy level and to maximize the electron injection in a SL-PhOLED. As investigating new electron-withdrawing fragments for SL-PhOLEDs is of great interest to contribute to the development of this promising simplified technology, this work shows that the DMB fragment might be then considered for future designs in this simplified OLED technology.

Supporting Information

Supporting Information is available from the Wiley Online Library or from the author.

Acknowledgements

This work has been supported by the ANR (N°19-CE05-0024- *SpiroQuest* Project). CB thanks the ADEME (Ecoelec Project, Dr Bruno Lafitte) for PhD grant. EJ and CP thank the Université de Rennes for the allocation of a Défi Scientifique 2023-Recherche transdisciplinaire interpoles. The author also thank the CRMPO (Rennes) for mass analyses. This work was granted access to the HPC resources of TGCC/CEA/CINES/IDRIS under the allocation 2024 AD010814136R1 awarded by GENCI. The authors acknowledge NanoRennes for the technological support, a platform affiliated to RENATECH+ (the French national facilities network for micro-nanotechnology).

Conflict of Interest

The authors declare no conflict of interest.

Data Availability Statement

The data that support the findings of this study are available from the corresponding author upon reasonable request.

Keywords

bipolar host material, single-layer phosphorescent OLED, spiro compounds, yellow emission

Received: June 28, 2024
Revised: September 7, 2024
Published online:

[1] C. W. Tang, S. A. VanSlyke, *Appl. Phys. Lett.* **1987**, *51*, 913.
[2] M. A. Baldo, D. F. O'Brien, Y. You, A. Shoustikov, M. E. Thompson, S. Sibley, *Nature* **1998**, *395*, 151.
[3] G. Hong, X. Gan, C. Leonhardt, Z. Zhang, J. Seibert, J. M. Busch, S. Bräse, *Adv. Mater.* **2021**, *33*, 2005630.
[4] M. A. Baldo, D. F. O'Brien, M. E. Thompson, S. R. Forrest, *Phys. Rev. B.* **1999**, *60*, 14422.
[5] M. A. Baldo, C. Adachi, S. R. Forrest, *Phys. Rev. B.* **2000**, *62*, 10967.
[6] C. Adachi, M. A. Baldo, M. E. Thompson, S. R. Forrest, *J. Appl. Phys.* **2001**, *90*, 5048.
[7] C. Poriel, J. Rault-Berthelot, *Acc. Mater. Res.* **2022**, *3*, 379.
[8] Y. Wang, J. H. Yun, L. Wang, J. Y. Lee, *Adv. Funct. Mater.* **2020**, *31*, 2008332.
[9] D. Li, J. Li, D. Liu, W. Li, C.-L. Ko, W.-Y. Hung, C. Duan, *ACS Appl. Mater. Interfaces* **2021**, *13*, 13459.
[10] Q.-L. Xu, X. Liang, S. Zhang, Y.-M. Jing, X. Liu, G.-Z. Lu, Y.-X. Zheng, J.-L. Zuo, *J. Mater. Chem. C.* **2015**, *3*, 3694.
[11] W. Song, Q. Xu, J. Zhu, Y. Chen, H. Mu, J. Huang, J. Su, *ACS Appl. Mater. Interfaces* **2020**, *12*, 19701.
[12] X. Tang, X.-Y. Liu, Y. Yuan, Y.-J. Wang, H.-C. Li, Z.-Q. Jiang, L.-S. Liao, *ACS Appl. Mater. Interfaces* **2018**, *10*, 29840.
[13] W.-C. Chen, Y. Yuan, Z.-L. Zhu, Z.-Q. Jiang, S.-J. Su, L.-S. Liao, C.-S. Lee, *Chem. Sci.* **2018**, *9*, 4062.
[14] K. Udagawa, H. Sasabe, C. Cai, J. Kido, *Adv. Mater.* **2014**, *26*, 5062.
[15] C. Poriel, J. Rault-Berthelot, Z.-Q. Jiang, *Mater. Chem. Front.* **2022**, *6*, 1246.
[16] D. Ari, Y.-J. Yang, C. Quinton, Z.-Q. Jiang, D.-Y. Zhou, C. Poriel, *Angew. Chem., Int. Ed.* **2024**, *63*, e202403066.
[17] C. Poriel, J. Rault-Berthelot, *Adv. Funct. Mat.* **2020**, *30*, 1910040.
[18] A. L. Fischer, K. E. Linton, K. T. Kamtekar, C. Pearson, M. R. Bryce, M. C. Petty, *Chem. Mater.* **2011**, *23*, 1640.
[19] K. E. Linton, A. L. Fischer, C. Pearson, M. A. P. Fox, L.-O. Palsson, M. R. Bryce, M. C. Petty, *J. Mater. Chem.* **2012**, *22*, 11816.
[20] A. Yoshii, Y. Onaka, K. Ikemoto, T. Izumi, S. Sato, H. Kita, H. Taka, H. Isobe, *Chem. Asian J.* **2020**, *15*, 2181.
[21] F. Lucas, O. A. Ibraikulov, C. Quinton, L. Sicard, T. Heiser, D. Tondelier, B. Geffroy, N. Leclerc, J. Rault-Berthelot, C. Poriel, *Adv. Opt. Mater.* **2020**, *8*, 1901225.
[22] F. Lucas, C. Quinton, S. Fall, T. Heiser, D. Tondelier, B. Geffroy, N. Leclerc, J. Rault-Berthelot, C. Poriel, *J. Mater. Chem. C.* **2020**, *8*, 16354.
[23] C. Poriel, J. Rault-Berthelot, *Adv. Funct. Mater.* **2021**, *31*, 2010547.
[24] F. Lucas, C. Brouillac, S. Fall, N. Zimmerman, D. Tondelier, B. Geffroy, N. Leclerc, T. Heiser, C. Lebreton, E. Jacques, C. Quinton, J. Rault-Berthelot, C. Poriel, *Chem. Mater.* **2022**, *34*, 8345.

[25] C. Brouillac, F. Lucas, D. Ari, D. Tondelier, J. Meot, M. Malvaux, C. Jadaud, C. Lebreton, J. Rault-Berthelot, C. Quinton, E. Jacques, C. Poriel, *Adv. Electron. Mater* **2024**, *10*, 2300582.
[26] C. Zang, X. Peng, H. Wang, Z. Yu, L. Zhang, W. Xie, H. Zhao, *Org. Electron.* **2017**, *50*, 106.
[27] Y. Yin, X. Wen, J. Yu, L. Zhang, W. Xie, *IEEE Photon. Technol. Lett.* **2013**, *25*, 2205.
[28] Z. Wu, Z. Yang, K. Xue, C. Fei, F. Wang, M. Yan, H. Zhang, D. Ma, W. Huang, *RSC Adv.* **2018**, *8*, 11255.
[29] O. Sachnik, Y. Li, X. Tan, J. J. Michels, P. W. M. Blom, G. A. H. Wetzelaer, *Adv. Mater.* **2023**, *35*, 2300574.
[30] N. B. Kotadiya, P. W. M. Blom, G.-J. A. H. Wetzelaer, *Nat. Photonics* **2019**, *13*, 765.
[31] O. Sachnik, Y. Ie, N. Ando, X. Tan, P. W. M. Blom, G.-J. A. H. Wetzelaer, *Adv. Mater.* **2024**, *36*, 2311892.
[32] F. Lucas, D. Tondelier, B. Geffroy, T. Heiser, O. A. Ibraikulov, C. Quinton, C. Brouillac, N. Leclerc, J. Rault-Berthelot, C. Poriel, *Mater. Chem. Front.* **2021**, *5*, 8066.
[33] H.-H. Chang, W.-S. Tsai, C.-P. Chang, N.-P. Chen, K.-T. Wong, W.-Y. Hung, S.-W. Chen, *Org. Electron.* **2011**, *12*, 2025.
[34] F.-M. Hsu, L.-J. Chien, K.-T. Chen, Y.-Z. Li, S.-W. Liu, *Org. Electron.* **2014**, *15*, 3327.
[35] Z. Liu, M. G. Helander, Z. Wang, Z. Lu, *Org. Electron.* **2009**, *10*, 1146.
[36] W.-Y. Hung, T.-C. Wang, H.-C. Chiu, H.-F. Chen, K.-T. Wong, *Phys. Chem. Chem. Phys.* **2010**, *12*, 10685.
[37] W. Y. Hung, T. C. Tsai, S. Y. Ku, L. C. Chi, K. T. Wong, *Phys. Chem. Chem. Phys.* **2008**, *10*, 5822.
[38] Y. Yin, X. Piao, Y. Li, Y. Wang, J. Liu, K. Xu, W. Xie, *Appl. Phys. Lett.* **2012**, *101*, 063306
[39] N. Lin, J. Qiao, L. Duan, L. Wang, Y. Qiu, *J. Phys. Chem. C.* **2014**, *118*, 7569.
[40] C. Poriel, J. Rault-Berthelot, *Acc. Mater. Res.* **2023**, *9*, 733.
[41] S. N. Zou, X. Chen, S. Y. Yang, S. Kumar, Y. K. Qu, Y. J. Yu, M. K. Fung, Z. Q. Jiang, L. S. Liao, *Adv. Opt. Mater.* **2020**, *8*, 2001074.
[42] C. Brouillac, F.-C. Kong, J. Rault-Berthelot, C. Quinton, Z.-Q. Jiang, C. Poriel, *Adv. Mater. Technol.* **2023**, *8*, 2300763.
[43] C. Brouillac, W.-S. Shen, J. Rault-Berthelot, O. Jeannin, C. Quinton, Z.-Q. Jiang, C. Poriel, *Mater. Chem. Front.* **2022**, *6*, 1803.
[44] W. Z. Yuan, S. Chen, J. W. Y. Lam, C. Deng, P. Lu, H. H. Y. Sung, I. D. Williams, H. S. Kwok, Y. Zhang, B. Z. Tang, *Chem. Commun.* **2011**, *47*, 11216.
[45] L. Chen, G. Lin, H. Peng, H. Nie, Z. Zhuang, P. Shen, S. Ding, D. Huang, R. Hu, S. Chen, F. Huang, A. Qin, Z. Zhao, B. Z. Tang, *J. Mater. Chem. C.* **2016**, *4*, 5241.
[46] L. Chen, C. Zhang, G. Lin, H. Nie, W. Luo, Z. Zhuang, S. Ding, R. Hu, S.-J. Su, F. Huang, A. Qin, Z. Zhao, B. Z. Tang, *J. Mater. Chem. C.* **2016**, *4*, 2775.
[47] H. Shi, D. Xin, X. Gu, P. Zhang, H. Peng, S. Chen, G. Lin, Z. Zhao, B. Z. Tang, *J. Mater. Chem. C.* **2016**, *4*, 1228.
[48] H. Shi, M. Li, D. Xin, L. Fang, J. Roose, H. Peng, S. Chen, B. Z. Tang, *Dyes Pigm.* **2016**, *128*, 304.
[49] X. Dong, M. Li, H. Shi, F. Cheng, J. Roose, B. Z. Tang, *Tetrahedron* **2016**, *72*, 2213.
[50] Y. Li, Z. Zhuang, G. Lin, Z. Wang, P. Shen, Y. Xiong, B. Wang, S. Chen, Z. Zhao, B. Z. Tang, *New. J. Chem.* **2018**, *42*, 4089.
[51] L. Chen, Y. Jiang, H. Nie, R. Hu, H. S. Kwok, F. Huang, A. Qin, Z. Zhao, B. Z. Tang, *ACS Appl. Mater. Interfaces* **2014**, *6*, 17215.
[52] L. Chen, Y. Jiang, H. Nie, P. Lu, H. H. Y. Sung, I. D. Williams, H. S. Kwok, F. Huang, A. Qin, Z. Zhao, B. Z. Tang, *Adv. Funct. Mater.* **2014**, *24*, 3621.
[53] H. Shi, J. Yang, X. Dong, X. Wu, P. Zhou, F. Cheng, M. M. F. Choi, *RSC Adv.* **2014**, *4*, 19418.
[54] H. Shi, Z. Gong, D. Xin, J. Roose, H. Peng, S. Chen, J. W. Y. Lam, B. Z. Tang, *J. Mater. Chem. C.* **2015**, *3*, 9095.
[55] J. Huo, H. Wang, S. Li, H. Shi, Y. Tang, B. Z. Tang, *Chem. Rec.* **2020**, *20*, 556.
[56] Y. Kitamoto, T. Namikawa, T. Suzuki, Y. Miyata, H. Kita, T. Sato, S. Oi, *Tetrahedron Lett.* **2016**, *57*, 4914.
[57] Y. Kitamoto, T. Namikawa, T. Suzuki, Y. Miyata, H. Kita, T. Sato, S. Oi, *Org. Electron.* **2016**, *34*, 208.
[58] Y.-K. Wang, S.-F. Wu, Y. Yuan, S.-H. Li, M.-K. Fung, L.-S. Liao, Z.-Q. Jiang, *Org. Lett.* **2017**, *19*, 3155.
[59] X.-L. Chen, J.-H. Jia, R. Yu, J.-Z. Liao, M.-X. Yang, C.-Z. Lu, *Angew. Chem., Int. Ed.* **2017**, *56*, 15006.
[60] A. Khan, Y.-K. Wang, C.-C. Huang, S. Kumar, M.-K. Fung, Z.-Q. Jiang, L.-S. Liao, *Org. Electron.* **2020**, *77*, 105520.
[61] Y. Kitamoto, T. Namikawa, D. Ikemizu, Y. Miyata, T. Suzuki, H. Kita, T. Sato, S. Oi, *J. Mater. Chem. C.* **2015**, *3*, 9122.
[62] Y. H. Lee, S. Park, J. Oh, J. W. Shin, J. Jung, S. Yoo, M. H. Lee, *ACS Appl. Mater. Interfaces* **2017**, *9*, 24035.
[63] M.-S. Lin, L.-C. Chi, H.-W. Chang, Y.-H. Huang, K.-C. Tien, C.-C. Chen, C.-H. Chang, C.-C. Wu, A. Chaskar, S.-H. Chou, H.-C. Ting, K.-T. Wong, Y.-H. Liu, Y. Chi, *J. Mater. Chem.* **2012**, *22*, 870.
[64] H. Shi, D. Xin, X. Dong, J.-x. Dai, X. Wu, Y. Miao, L. Fang, H. Wang, M. M. F. Choi, *J. Mater. Chem. C.* **2014**, *2*, 2160.
[65] H.-G. Jang, B. S. Kim, J. Y. Lee, S.-H. Hwang, *Dalton Trans.* **2014**, *43*, 7712.
[66] M.-M. Xue, C.-C. Huang, Y. Yuan, L.-S. Cui, Y.-X. Li, B. Wang, Z.-Q. Jiang, M.-K. Fung, L.-S. Liao, *ACS Appl. Mater. Interfaces* **2016**, *8*, 20230.
[67] C. Wang, Y. Yuan, S.-Y. Li, Z.-B. Sun, Z.-Q. Jiang, C.-H. Zhao, *J. Mater. Chem. C.* **2016**, *4*, 7607.
[68] L. Zuo, G. Han, R. Sheng, K. Xue, Y. Duan, P. Chen, Y. Zhao, *RSC Adv.* **2016**, *6*, 55017.
[69] D. Tomkute-Luksiene, J. Keruckas, T. Malinauskas, J. Simokaitiene, V. Getautis, J. V. Grazulevicius, D. Volyniuk, V. Cherpak, P. Stakhira, V. Yashchuk, V. Kosach, G. Luka, J. Sidaravicius, *Dyes Pigm.* **2013**, *96*, 278.
[70] C.-H. Chen, W.-S. Huang, M.-Y. Lai, W.-C. Tsao, J. T. Lin, Y.-H. Wu, T.-H. Ke, L.-Y. Chen, C.-C. Wu, *Adv. Funct. Mater.* **2009**, *19*, 2661.
[71] M.-Y. Lai, C.-H. Chen, W.-S. Huang, J. T. Lin, T.-H. Ke, L.-Y. Chen, M.-H. Tsai, C.-C. Wu, *Angew. Chem., Int. Ed.* **2008**, *47*, 581.
[72] M. Romain, D. Tondelier, B. Geffroy, A. Shirinskaya, O. Jeannin, J. Rault-Berthelot, C. Poriel, *Chem. Commun.* **2015**, *51*, 1313.
[73] N. Mataga, Y. Kaifu, M. Koiz, *Bull. Chem. Soc. Jpn.* **1956**, *29*, 465.
[74] T.-C. Li, R.-C. Chang, *Int. J. of Precis. Eng. and Manuf.-Green Tech.* **2014**, 329.
[75] A. Turak, *Electron. Mater.* **2021**, *2*, 198.